

Parametric optimization of a coupled system integrating solid oxide fuel cell and graphene thermionic energy converter

Tianjun Liao^{a, b}, Yawen Dai, Chun Cheng, Qijiao He, Qidong Xu, Meng Ni^{a*}

^a *Department of Building and Real Estate, Hong Kong Polytechnic University, Hung Hom, Kowloon, Hong Kong, China*

^b *Department of Physics and Energy, Chongqing University of Technology, Chongqing 400054, China*

Abstract: In this work, a high-efficiency coupled system by integrating solid oxide fuel cell with graphene thermionic energy converter is proposed and evaluated. Based on theories of the electrochemistry, thermionic emission, heat transfer, and first law of thermodynamics, the formulas for the overall power density and energy conversion efficiency of the proposed system are derived, and the thermal and electrical characteristics of the coupled system are studied. The three special states such as ideal heat transfer, opened graphene thermionic energy converter, and shorted solid oxide fuel cell are discussed. The maximum power density and efficiency and the corresponding optimal conditions are determined. As the **subsystems** work independently, the dependences of the electrical parameters on **the temperature of the solid oxide fuel cell**, the current density **of the graphene thermionic energy converter**, and the coupled system's power density and efficiency are given, and the parametric optimal designs are presented. The effects of work function on the optimal performances are revealed. The results obtained in this work are of great significance to design and optimize the coupled energy cascade utilization system.

Key words: Solid oxide fuel cell; Graphene thermionic energy converter; Coupled system; Parametric optimization; Waste heat recovery

*Corresponding author (M. Ni)

Email: meng.ni@polyu.edu.hk; Tel: 852-27664152; Fax: 852-27645131

Nomenclature	
A_E	revised AD constant ($A \cdot \text{cm}^{-2} \cdot \text{K}^{-3}$)
A_C	conventional RD constant ($A \cdot \text{cm}^{-2} \cdot \text{K}^{-2}$)
C	isobaric molar heat capacity ($\text{eV} \cdot \text{mol}^{-1} \cdot \text{K}^{-1}$)
d	thickness of thermal interface material (cm)
e	elementary positive charge (C)
F	Faraday's constant ($\text{C} \cdot \text{mol}^{-1}$)
Δg	molar Gibbs energy ($\text{eV} \cdot \text{mol}^{-1}$)
Δh	molar enthalpy change ($\text{eV} \cdot \text{mol}^{-1}$)
$-\Delta \dot{H}$	enthalpy change (eV)
J	current density ($A \cdot \text{cm}^{-2}$)
$J_{e,a}$	exchange current density of anode ($A \cdot \text{cm}^{-2}$)
$J_{e,c}$	exchange current density of cathode ($A \cdot \text{cm}^{-2}$)
$J_{L,a}$	limiting current density of anode ($A \cdot \text{cm}^{-2}$)
$J_{L,c}$	limiting current density of cathode ($A \cdot \text{cm}^{-2}$)
k_B	Boltzmann constant ($\text{eV} \cdot \text{K}^{-1}$)
κ	thermal conductivity ($\text{W} \cdot \text{cm}^{-1} \cdot \text{K}^{-1}$)
l_v	Latent heat of phase change of water ($\text{eV} \cdot \text{mol}^{-1}$)
L_a	anode thickness (cm)
L_c	cathode thickness (cm)
L_e	electrolyte thickness (cm)
N	number of electrons transferred in reaction
P	power density ($\text{W} \cdot \text{cm}^{-2}$)
p_i	partial pressure (atm)
q_j	heat flow (W)
r	resistance (Ω)
R	universal gas constant ($\text{J} \cdot \text{mol}^{-1} \cdot \text{K}^{-1}$)
S	area (cm^2)
T	temperature (K)
T_b	boiling point of water (K)
U	heat transfer coefficient ($\text{W} \cdot \text{cm}^{-2} \cdot \text{K}^{-1}$)
V	voltage (V)
$E_{\text{fer},E}$	Fermi level of emitter (eV)
$E_{\text{fer},C}$	Fermi level of collector (eV)
Greek symbols	
α	area ratio between two subsystems
β	resistance ratio
σ	electric conductivity ($\text{S} \cdot \text{cm}^{-1}$)
δ	Stefen-Boltzmann constant ($\text{W} \cdot \text{cm}^{-2} \cdot \text{K}^{-4}$)
ψ_E	work function of emitter (eV)
ψ_C	work function of collector (eV)
η	efficiency
ε	thermal emissivity
Subscript	
a	anode
A	ambient
b	boiling point
c	cathode
C	collector
e	electrolyte
E	emitter
F	fuel cell
i	H_2 , O_2 , H_2O
L	limit
I	internal
j	in, out, R, E, C
act	activation overpotential
con	concentration overpotential
lb	low bound
leak	leakage resistance
max	maximum
ohm	ohmic overpotential
P	maximum power density point
ub	up bound
R	radiative
Rev	reversible voltage
T	thermionic
Abbreviations	
GTEC	graphene thermionic energy converter
FC	fuel cell
FFTC	far-field thermophotovoltaic cell
NFTC	near-field thermophotovoltaic cell
RD	Richardson-Dushman
SOFC	solid oxide fuel cell
TEC	thermionic energy converter

1. Introduction

Fuel cell (FC) is an energy conversion device that continuously converts the chemical energy in fuel and oxidant into clean electricity [1]. Especially, high temperature solid oxide FC (SOFC) can reform carbon-based fuel within the FCs and have wide adaptability for various hydrocarbons fuel [2-4]. However, the high-grade waste heat emission from the SOFCs needs to be effectively utilized to enhance the overall energy efficiency [5]. One of the solutions is that we can establish energy cascade utilization systems by coupling SOFC with solid-state energy converters such as thermoelectric devices [6-8], far-field thermophotovoltaic cells (FFTCs) [7], near-field thermophotovoltaic cells (NFTCs) [10], thermionic energy converters (TECs) [11-13], etc. Due to small size, large power density, and high energy conversion efficiency, the TECs are applied to military, aerospace and other fields and can be driven by the thermal energy, solar energy, and nuclear energy by means of thermionic emission [14, 15]. The previous works demonstrated that the TECs can efficiently recycle waste heat from the SOFC [11-13], direct carbon FC [16], and molten carbonate FC [17]. Therefore, the development of high-efficiency thermal-to-electricity conversion devices is of great significance to the recovery of waste heat from high-temperature FCs. Based on the novel optical, electrical, and mechanical properties, graphene material can be applied in the fields of energy conversion and storage [18]. Liang *et al.* [19] and Mishra [20] selected graphene as emitter material to propose a new model of graphene TEC (GTEC), studied the thermionic emission mechanisms of single-layer graphene, and derived the formulas for the power density and efficiency. Mishra [21] further studied the theoretical model of the thermionic emission of multilayer graphene and demonstrated the feasibility of multilayer GTEC. Liang *et al.* [22] designed a van der Waals heterostructure GTEC. It was found that the device can achieve high energy conversion efficiency in the range of 400 to 500 K.

In the previous works related SOFC coupled systems [11-13], the relationship between the

subsystems' matching area ratio and the electrical parameters is constrained by the energy balance equation. The subsystems' parameters are optimized to obtain the maximum power density. Nevertheless, the system's performances depend on the finite-time heat transfer losses and thermo-electric coupling losses. Therefore, it is of great significance to integrate the SOFC with the novel GTEC by considering the multiple irreversible factors. In this work, a high-efficiency coupled system by integrating SOFC and GTEC is established. The impacts of irreversible factors on the operation of the coupled system are considered. The expressions for power density and efficiency of the coupled system are derived. The parametric optimal design strategies are provided for the recovery of the waste heat released from the high temperature FC.

2. Model descriptions

The SOFC-NFTC coupled system consisting of an SOFC, a regenerator, and a GTEC is shown in Fig. 1(a). Within the GTEC, the emitter at temperature T_E and the collector at temperature T_C separated by a vacuum gap can exchange radiative heat flow q_r [19, 20]. Graphene covers the surface of tungsten to form an emitter [19, 20]. The tungsten is coated with negative electron affinity material to form a collector [15, 19, 20]. The GTEC's emitter contacts the SOFC through a thermally conductive material to operate at a high temperature. The regenerator preheats the incoming fuel and air by means of the high-temperature exhaust gas of the SOFC and the waste heat from the collector [9, 10]. The working mechanism of coupled system is that the electrons inside the emitter obtain thermal energy to escape from the surface, and then are absorbed by the collector through a vacuum gap [23]. As a result, the net electron flow will return to the emitter through a load and achieve energy conversion process. Because of the thermal electrons and the radiative heat transfers, the temperature of the collector is raised to generate the reverse thermionic emission current density [23]. Thus, the back surface of the collector releases the heat flow q_{out} into the environment [23]. The energy band diagram of GTEC is

presented in Fig. 1(b). ψ_E and ψ_C are the work functions of the emitter and the collector, respectively [19]. $E_{\text{Fer,E}}$ and $E_{\text{Fer,C}}$ are the Fermi levels of the graphene and the tungsten, respectively [18]. The differences between the vacuum and the respective Fermi level determine the two electrodes' work functions ψ_E and ψ_C . The voltage V_T of the GETC is equal to $(E_{\text{Fer,E}} - E_{\text{Fer,C}})/e$ [23]. According to the reasonable selection of vacuum gap, the impacts of the space charge effect on the GTEC can be neglected [19]. The work function of the intrinsic graphene is equal to 4.514 eV, which can be tuned by coating negative electron affinity material (e.g. cesium) [19].

2.1. The power output and efficiency of an SOFC

According to the irreversible thermodynamic model of an SOFC, the power output density P_F depends on the current density J_F , the reversible voltage V_{Rev} , and the irreversible voltage losses including the ohmic overpotential V_{ohm} , concentration overpotential V_{con} , and activation overpotential V_{act} . Based on the above descriptions, the expressions for efficiency η_F and power density P_F are, respectively, presented as [9-11, 13, 24-25]

$$\eta_F = \frac{P_F}{-\Delta \dot{H}} \quad (1)$$

and

$$P_F = V_F J_F \left[1 - \beta V_F / (V_{\text{act}} + V_{\text{con}} + V_{\text{ohm}}) \right], \quad (2)$$

where $\beta = r_1 / r_{\text{Leak}} = 10^{-3}$. $r_1 = (V_{\text{act}} + V_{\text{con}} + V_{\text{ohm}}) / (J_F S_F)$ is the internal resistance caused by three overpotentials [13]. r_{Leak} describes the leakage resistance in parallel with the load circuit [13]. S_F is the surface area of the contact electrode. $V_F = V_{\text{Rev}} - V_{\text{act}} - V_{\text{con}} - V_{\text{ohm}}$ is the output voltage [24, 25]. $-\Delta \dot{H} = -\Delta h J_F / (NF)$ represents the total enthalpy change for electrochemical reaction. $N=2$ means the number of electrons transferred in reaction. $F = 9.65 \times 10^4 \text{ C} \cdot \text{mol}^{-1}$ stands for the Faraday's constant. Δh stands for the molar enthalpy change for electrochemical reaction, which can be expressed as [26]

$$(\Delta h)_T = h_{298}^0 + \int_{298}^{T_b} C_{p,H_2O(L)} dT + l_v + \int_{T_b}^T C_{p,H_2O(g)} dT - \int_{298}^{T_b} C_{p,H_2} dT - \frac{1}{2} \int_{298}^T C_{p,O_2} dT, \quad (3)$$

where $C_{p,H_2} = 27.28 + 0.00326T_F + 50000T_F^{-2}$, $C_{p,O_2} = 29.96 + 0.00418T_F - 167000T_F^{-2}$, $C_{p,H_2O(L)} = 75.44 \text{ J} \cdot \text{K}^{-1} \cdot \text{mol}^{-1}$, and $C_{p,H_2O(g)} = 30.00 + 0.01071T_F + 33000T_F^{-2}$, are, respectively, the isobaric molar heat capacities of liquid water, water vapor, hydrogen, and oxygen. l_v is latent heat of phase change of water. T_b is boiling point of water.

According to the Nernst equation, the reversible voltage V_{Rev} is given by [9-11]

$$V_{\text{Rev}} = \frac{RT_F}{NF} \ln \left(\frac{p_{H_2} \sqrt{p_{O_2}}}{p_{H_2O}} \right) - \frac{\Delta g(T_F)}{NF}, \quad (4)$$

where $R = 8.314 \text{ J} \cdot \text{mol}^{-1} \cdot \text{K}^{-1}$ is the universal gas constant. $\Delta g(T_F)$ means the molar Gibbs energy change under the standard atmospheric pressure. p_{H_2} , p_{O_2} , and p_{H_2O} are, respectively, the partial pressures of the hydrogen, oxygen, and water. The ohmic overpotential V_{ohm} can be calculated as [27]

$$V_{\text{ohm}} = J_F \left(\frac{L_a}{\sigma_a} + \frac{L_c}{\sigma_c} + \frac{L_e}{\sigma_e} \right), \quad (5)$$

where $L_a = 5.0 \times 10^{-2} \text{ cm}$, $L_c = 5.0 \times 10^{-2} \text{ cm}$, and $L_e = 5.0 \times 10^{-2} \text{ cm}$ are the thicknesses of the anode, cathode, and electrolyte. $\sigma_a = 9.5 \times 10^7 T_F^{-1} \exp(-1150/T_F)$, $\sigma_c = 4.2 \times 10^7 T_F^{-1} \exp(-1200/T_F)$, and $\sigma_e = 3.34 \times 10^4 \exp(-10300/T_F)$ are the electric conductivities. The activation overpotential V_{act} is expressed as [9-11]

$$V_{\text{act}} = \frac{RT_F}{F} \left[\sinh^{-1} \left(\frac{J_F}{2J_{e,a}} \right) + \sinh^{-1} \left(\frac{J_F}{2J_{e,c}} \right) \right], \quad (6)$$

where $J_{e,a}$ and $J_{e,c}$ are, respectively, the exchange current densities of the anode and cathode.

The concentration overpotentials V_{con} can be expressed as [9-11]

$$V_{\text{con}} = -\frac{RT}{NF} \left[\ln \left(1 - \frac{J_F}{J_{L,a}} \right) + \ln \left(1 - \frac{J_F}{J_{L,c}} \right) \right], \quad (7)$$

where $J_{L,a}$ and $J_{L,c}$ denotes the limited current densities of the anode and cathode, respectively.

2.2. The power output of a GTEC

As the GTEC is in operation, the power density P_T is computed as [23, 28]

$$P_T = q_{in} - q_{out} = V_T J_T, \quad (8)$$

where $V_T = (\psi_E - \psi_C)/e$ is the GTEC' output voltage. $J_T = J_E - J_C$ is the net current density. J_E and J_C are the current densities emitted from the cathode and the anode.

According to the thermionic emission theory, the current density J_E excited from the emitter surface is determined by the revised Richardson-Dushman (RD) equation [19]

$$J_E = A_E T_E^3 \exp\left[-(\psi_E - E_{\text{Fer},E})/(k_B T_E)\right], \quad (9)$$

where k_B is the Boltzmann constant. $E_{\text{Fer},E} = 0.80\text{eV}$ is chosen. $A_E = 0.01158\text{A} \cdot \text{cm}^{-2} \cdot \text{K}^{-3}$ is the revised AD constant.

The current density J_E excited from the collector surface is determined by the conventional RD equation, i.e., [23, 28]

$$J_C = A_C T_C^2 \exp\left[-\psi_C/(k_B T_C)\right], \quad (10)$$

where $A_C = 120\text{A} \cdot \text{cm}^{-2} \cdot \text{K}^{-2}$ is the conventional RD constant.

When the vacuum gap is larger than the thermal wavelength governed by the Wien's displacement law, the heat transfer within the two electrodes obeys far-field radiative mechanism. According to Fig. 1(a) and the first law of thermodynamics, the energy balance equations related to the GTEC's two electrodes can be expressed as [28]

$$q_{in} = q_E + q_R \quad (11)$$

and

$$q_{out} = q_C + q_R \quad (12)$$

where $q_R = \varepsilon \delta (T_E^4 - T_C^4)$ is the radiative loss between the two electrodes. $\varepsilon = (\varepsilon_E^{-1} + \varepsilon_C^{-1} - 1)^{-1} = 0.05$ is effective thermal emissivity between the two electrodes. $\varepsilon_E = 0.06$ and $\varepsilon_C = 0.30$ are the thermal emissivities of the two electrodes. $\delta = 5.67 \times 10^{-12} \text{W} \cdot \text{m}^{-2} \cdot \text{K}^{-4}$ is the Stefan-Boltzmann constant.

Based on the Refs. [22, 28], the two heat flows q_E and q_C are listed as

$$q_E = [J_E(\psi_E + 3k_B T_E) - J_C(\psi_E + 2k_B T_C)] / e \quad (13)$$

and

$$q_C = [J_E(\psi_C + 3k_B T_E) - J_C(\psi_C + 2k_B T_C)] / e, \quad (14)$$

where $(\psi_E + 3k_B T_E)$ and $(\psi_C + 2k_B T_C)$ are the heat flow rates carried by each electron escaping from the electrodes' surface. $(\psi_C + 3k_B T_E)$ is the heat flow rate carried by each electron from the emitter to the collector. $(\psi_E + 2k_B T_C)$ is the heat flow rate of the each electron emitting from the collector surface to the emitter. $3k_B T_E$ and $2k_B T_C$ are the average thermal kinetic energy of the each electron in the two electrodes after crossing the barrier.

2.3 The power output and efficiency of the coupled system

According to the first law of thermodynamics, an energy balance equation is determined as:

$$-\Delta\dot{H} - P_F = q_{in}. \quad (15)$$

It is assumed that the heat flow transfers between the of GTEC and the respective heat reservoirs obey Newton's cooling law, two equations are given by [24, 28]

$$q_{in} = U_E (T_F - T_E), \quad (16)$$

and

$$q_{out} = U_C (T_C - T_A) \quad (17)$$

where $U_E = \kappa_E / d_E$ and $U_C = \kappa_C / d_C$ are the heat transfer coefficients [22]. κ and d are the thermal conductivity and thickness of thermal interface material, respectively. For given the related parameters such as V_F , V_T , T_A , Eqs. (2)-(17) can be solved to obtain the temperatures T_F , T_E , and T_C .

Based on Eqs. (1), (2), and (14), the total power density and overall energy conversion efficiency of the SOFC-GTEC coupled system can be derived as

$$P = P_F + P_T = V_F J_F [1 - \beta V_F / (V_{act} + V_{con} + V_{ohm})] + V_T (J_E - J_C) \quad (18)$$

and

$$\eta = \frac{P}{-\Delta\dot{H}} = \frac{V_F J_F \left[1 - \beta V_F / (V_{act} + V_{con} + V_{ohm}) \right] + V_T (J_E - J_C)}{-\Delta h J_F / (NF)}. \quad (19)$$

Equations (1)-(19) can be directly used to analyze the parametric optimization of the coupled system.

The performance parameters of the system are listed in Table 1.

3. Parametric optimization

3.1. The cases of ideal heat transfer

When $U_E = U_C \rightarrow \infty$, the Newton heat transfers between the GTEC's two electrodes and the heat reservoirs are neglected. The coupled system is simplified as a constant temperature heat source model, i.e., $T_E = T_F$ and $T_C = T_A$. Combining Eqs. (11)-(15), a thermal balance equation is derived as:

$$\alpha \left\{ -\Delta h J_F / (NF) - V_F J_F \left[1 - \beta V_F / (V_{act} + V_{con} + V_{ohm}) \right] \right\} = \left[J_E (\psi_E + 3k_B T_E) - J_C (\psi_E + 2k_B T_C) \right] / e + \varepsilon \delta (T_E^4 - T_C^4), \quad (20)$$

where $\alpha = S_F / S_T$ is the area ratio between the SOFC and the GTEC.

Through the area matching of the subsystems, the energy balance is achieved. By solving Eq. (20), the area ratio $\alpha = S_F / S_T$ can be obtained for given related parameters such as J_F , T_F , V_T , etc. According to optimize the voltage V_T , the curves of the maximum power density P_{max} and the maximum efficiency η_{max} varying with temperature T_F are plotted in Fig. 2(a). It is seen from Fig. 2(a) that the maximum power density P_{max} achieves an upper-bound value $P_{ub} = 1.10 \text{ W} \cdot \text{cm}^{-2}$, while the maximum efficiency η_{max} achieves a lower-bound value $\eta_{lb} = 0.817$ when $T_F = T_{F,up}$. As temperature operates in the region $T_F > T_{F,up}$, both P_{max} and η_{max} decreases with increasing T_F . In order to present the high performances of the coupled system, the temperature T_F should locate in the region:

$$T_F \leq T_{F,up}. \quad (21)$$

In above region, a maximum value of $(P_{max} \times \eta_{max})$ can be obtained, and thus, the coupled system can

deliver large electricity and exhibit high efficiency.

Based on Eq. (21), the efficiency should be situated in the region of:

$$\eta_{\max} \geq \eta_{\text{lb}}. \quad (22)$$

Fig. 2(b) shows that the optimized voltage $V_{\text{T,P}}$ at the maximum power density is close to the optimized voltage $V_{\text{T},\eta}$ at the maximum efficiency. The optimized voltages $V_{\text{T,P}}$ and $V_{\text{T},\eta}$ are equal to $V_{\text{T,up}}$ when $T_{\text{F}} = T_{\text{F,up}}$. Thus, the voltage V_{T} should be situated in the region of:

$$V_{\text{T}} \leq V_{\text{T,up}}. \quad (23)$$

Fig. 2(c) shows that the curves of the optimized current density $J_{\text{F,P}}$ at the maximum power density and the optimized current density $J_{\text{F},\eta}$ at the maximum efficiency as a function of T_{F} . The optimized current density $J_{\text{F,P}}$ achieves an upper-bound value $J_{\text{F,ub}}$ as $T_{\text{F}} = T_{\text{F,up}}$, while current density $J_{\text{F},\eta}$ is a monotonic increasing function of T_{F} . Thus, the current density J_{F} should be situated in:

$$J_{\text{F}} \leq J_{\text{F,ub}}. \quad (24)$$

Fig. 2(d) shows that the optimized area ratio α_{p} at the maximum power density and the optimized area ratio α_{η} at the maximum efficiency are monotonic increasing functions of T_{F} . The optimized area ratio α_{p} is small than the optimized area ratio α_{η} due to $J_{\text{F,P}} \geq J_{\text{F},\eta}$.

3.2. The case of GTEC is opened

Because the coupled system is difficult for designing and fabricating as $\alpha \neq 1$. For convenient discussion, the area ratio $\alpha = 1$ is chosen in the following discussions. Through the adjustment of electrical parameters of the subsystems, the energy balance is achieved. When the GTEC is opened, i.e., $\text{Load} \rightarrow \infty$ and $J_{\text{T}} \rightarrow 0$, it can't generate electricity and only acts as a cooler to transfer the waste heat from the SOFC to the environment. For given current density J_{F} , the temperature T_{F} of the SOFC and the open-circuit voltage $V_{\text{T,oc}}$ can be obtained by solving Eqs. (1)-(18). The power output density P and the efficiency η can be further calculated, as shown in Fig. 3(a). It is found from Fig.

3(a) that one can obtain the maximum power density $P_{\max} = 0.765 \text{ W} \cdot \text{cm}^{-2}$ and maximum efficiency $\eta_{\max} = 0.580$, and the corresponding optimal current densities $J_{F,P} = 1.34 \text{ A} \cdot \text{cm}^{-2}$ and $J_{F,\eta} = 0.631 \text{ A} \cdot \text{cm}^{-2}$. Using the optimal current densities $J_{F,P}$ and $J_{F,\eta}$, the optimal temperatures $T_{F,P}$ and $T_{F,\eta}$ can be determined. Due to the irreversible heat loss during the electrochemical process in SOFC, $J_{F,P}$ is larger than $J_{F,\eta}$. In order to make the power and efficiency as large as possible, the current density J_F and the temperature T_F should be located in the following regions:

$$J_{F,\eta} \leq J_F \leq J_{F,P} \quad (25)$$

and

$$T_{F,\eta} \leq T_F \leq T_{F,P}, \quad (26)$$

In Fig. 3(b), the temperature T_F of the SOFC and the open-circuit voltage $V_{T,oc}$ increases with increases of J_F . Because the waste heat rate $(-\Delta\dot{H} - P_F)$ increases as J_F increases, the finite-time heat transfer between the SOFC and the GTEC's emitter leads that T_F is increased. On the other hand, the open-circuit voltage $V_{T,oc}$ should be increased to maintain the energy balances, i.e., Eqs. (11)-(17).

3.3. The case of SOFC is shorted

When the SOFC is opened, i.e., $\text{Load} \rightarrow \infty$ and $J_F = 0$, it can't generate electricity and waste heat flow. Similarly, the whole coupled system can't work normally. When the SOFC is shorted, i.e., $V_F = 0$, it can release waste heat and work as a heat source. The power output density P and the efficiency η can be further calculated, as shown in Fig. 4(a). It is observed from Fig. 4(a) that one can obtain a maximum power density $P_{\max} = 0.496 \text{ W} \cdot \text{cm}^{-2}$ and a maximum efficiency $\eta_{\max} = 0.176$ as $V_T = V_{T,P} = 0.951 \text{ V}$. Fig. 4(b) shows that as the output voltage V_T increases, the temperature T_F increases linearly and then remains unchanged, while the shorted current density $J_{F,SC}$ first remains unchanged and then decreases linearly. Making comparasions between Figs. 3(a) and 4(a), the performances of the single SOFC are better than those of the single GTEC.

3.3. The case of SOFC and GTEC simultaneously generate electricity

When $U_E = U_C \neq \infty$, the Newton heat transfers between the GTEC's two sides and the heat reservoir are non-ideal, i.e., $T_E < T_F$ and $T_C > T_A$. When the sub-systems don't operate at shorted and opened states, they can simultaneously generate electricity. Through numerically simulation, we can study the thermal and the electrical characteristics of the coupled system. The 3D graph of the temperature T_F varying with the voltage V_T and the current density J_F , as depicted in Fig. 5(a). It is seen from Fig. 5(a) that temperature T_F monotonically increases as the voltage V_T and the current density J_F increase, which are determined by the thermal balance equations. Fig. 5(b) shows that the current density J_F monotonically decreases with J_F . Figs. 5(c) and (d) show that there exists a maximum power density P_{\max} and a maximum efficiency η_{\max} . Because of the irreversible losses, P_{\max} and η_{\max} are obtained at different electrical parameters J_F and V_T .

In order to determine the parametric optimal regions, the optimal power density P_{opt} and efficiency η_{opt} can be obtained by optimizing the voltage V_T for given current density J_F . Fig. 6(a) shows that when $J_F = J_{F,P} = 1.88 \text{ A} \cdot \text{cm}^{-2}$ and $J_F = J_{F,\eta} = 0.628 \text{ A} \cdot \text{cm}^{-2}$, the optimal power density P_{opt} and efficiency η_{opt} can achieve their maximum values $P_{\max} = 1.01 \text{ W} \cdot \text{cm}^{-2}$ and $\eta_{\max} = 0.579$. Comparing the present work to the reported work [11], one can find that both the power and efficiency are further enhanced. Due to the novel electrical properties of graphene, its thermionic emission characteristics are superior to those of the traditional metal materials.

Using the data in Fig. 6(a), the performance characteristic curve of P as a function of η can be plotted, as shown in Fig. 6(b). Generally, the negative slope part in Fig. 6(b) is depicted when J_F locates in the region: $J_{F,\eta} \leq J_F \leq J_{F,P}$. According to the region $J_{F,\eta} \leq J_F \leq J_{F,P}$, the optimal regions of power density P and the efficiency η can be determined as:

$$P_{\max} \geq P > P_{\eta} \quad (27)$$

and

$$\eta_{\max} \geq \eta \geq \eta_p, \quad (28)$$

where P_η and η_p are the power density and the efficiency when $\eta = \eta_{\max}$ and $P = P_{\max}$, respectively.

The effects of the collector's work function ψ_c on the parametric optimal characteristics of the SOFC-GTEC coupled system are given in Table 2. It is seen from Table 2 that the effects of the collector's work function on the efficiency η_{\max} and the corresponding optimal voltage $V_{F,\eta}$ and temperature $T_{F,\eta}$ are negligible, while decreasing the collector's work function can improve the power density P_{\max} . Table 2 displays that the optimal temperature $T_{F,P}$ and the optimal voltage $V_{F,P}$ at P_{\max} decrease with decrease of ψ_c , while $V_{T,P}$ and $J_{F,P}$ increase as ψ_c decreases. The optimal temperature $J_{F,\eta}$ at η_{\max} increase with decrease of ψ_c , while $V_{T,\eta}$ at η_{\max} increase with decrease of ψ_c . It is worthy for mentioning that Table 2 doesn't indicated that the performances can be greatly improved as we further decrease ψ_c , because the present material technology can only decrease the tungsten' work function to 1.50 eV [29, 30]. Making comparison between Fig. 2(a) and Table 2, the maximum power density P_{\max} of non-ideal system is smaller than that of the ideal system, which indicate that the irreversible factors in the system can't be neglected. Making comparison between Fig. 3(a) and Table 2, one can find that integrating GTEC with the SOFC is significant for enhancing the power density.

In addition, graphene covered on the surface of the tungsten forms a Schottky barrier height, which may impact on the system's performance. The discussion the above key issue is beneficial to design of the actual system.

5. Conclusions

A new electricity generation hybrid system consisting of an SOFC and a GTEC has been proposed and theoretically optimized. The main results are listed as follows:

(1) The ideal heat transfer-based coupled system is studied. Through area matching and parametric optimal analysis, upper-bound power density $P_{ub} = 1.10 \text{ W} \cdot \text{cm}^{-2}$ and the while lower-bound efficiency $\eta_{lb} = 0.817$ are achieved.

(2) As the GTEC is opened, the maximum power density $P_{max} = 0.765 \text{ W} \cdot \text{cm}^{-2}$ and maximum efficiency $\eta_{max} = 0.580$, and the corresponding optimal current densities $J_{F,P} = 1.34 \text{ A} \cdot \text{cm}^{-2}$ and $J_{F,\eta} = 0.631 \text{ A} \cdot \text{cm}^{-2}$ are determined.

(3) As the SOFC is shorted, the maximum power density $P_{max} = 0.496 \text{ W} \cdot \text{cm}^{-2}$ and maximum efficiency $\eta_{max} = 0.176$ as $V_T = 0.951 \text{ V}$ are calculated.

(4) As the irreversible Newton heat transfer is considered, the maximum power density $P_{max} = 1.01 \text{ W} \cdot \text{cm}^{-2}$ and maximum efficiency $\eta_{max} = 0.579$, and the corresponding optimal current densities $J_{F,P} = 1.88 \text{ A} \cdot \text{cm}^{-2}$ and $J_{F,\eta} = 0.628 \text{ A} \cdot \text{cm}^{-2}$ are obtained.

The results show that although the maximum power density of non-ideal system is smaller than that of the ideal system, the coupled system is significant for enhancing the power density compared to the single SOFC and GTEC. The proposed model in present work can be applied to waste heat recovery and performance enhancement of the tubular SOFC [31].

Acknowledgements

This work has been supported by the Science and Technology Research Program of Chongqing Municipal Education Commission (Grant No. KJQN201901144) and the Scientific Research Foundation of Chongqing University of Technology (Grant No. 2019ZD22), People's Republic of China. M. Ni thanks the grants (Project Number: PolyU 152214/17E and PolyU 152064/18E) from Research Grant Council, University Grants Committee, Hong Kong SAR.

References

- [1] P. Boldrin, N. P. Brandon, *Nature Catalysis* 2 (2019) 571.
- [2] Q. Wang, L. Li, C. Wang, *J. Power Sources* 452 (2020) 399–407.
- [3] D. Papurello, V. Chiodo, S. Maisano, A. Lanzini, M. Santarelli, *Renew. Energy* 127 (2018) 481–494.
- [4] A. Lanzini, P. Leone. *Int. J. Hydrogen Energy* 35 (2010) 2463–76.
- [5] X. J. Luo, K. F. Fong, *J. Power Sources*, 429 (2019) 127–148.
- [6] Z. Yang, T. Liao, B. Lin, *Sci. Sin. Tech.*, 44 (2014) 569–580.
- [7] H. Zhang, H. Xu, B. Chen, F. Dong, M. Ni, *Energy* 132 (2017) 280–288.
- [8] H. Zhang, W. Kong, F. Dong, H. Xu, B. Chen, M. Ni, *Energy Convers. Manage* 148 (2017) 1382–1390.
- [9] T. Liao, L. Cai, Y. Zhao, J. Chen, *J. Power Sources* 306 (2016) 666–673.
- [10] T. Liao, Q. He, Q. Xu, Y. Dai, C. Cheng, M. Ni, *J. Power Sources* 452 (2020) 227831.
- [11] Y. Wang, L. Cai, T. Liu, J. Wang, *Chen J, Energy* 93 (2015) 900–907.
- [10] H. Zhang, J. Wang, F. Wang, J. Zhao, H. Miao, J. Yuan, *Energy Convers. Manage.* 193 (2019) 64–73.
- [12] Z. Yang, T. Liao, B. Lin, *Sci. Sin. Tech.* 44 (2014) 1173–1184.
- [13] Y. Deng, B. Qiu, K. Lu, Y. Yin, X. Gong, B. Pang, X. Huang, Y. Li, Y. Wu, G. Su, *Appl. Therm. Engineering* 173 (2020) 115237.
- [15] G. Xiao, G. Zheng, D. Ni, Q. Li, M. Qiu, M. Ni, *Applied Energy* 223 (2018) 134–145.
- [16] H. Xu, B. Chen, P. Tan, W. Cai, Y. Wu, H. Zhang, M. Ni, *Appl. Energy* 226 (2018) 881–890.
- [17] C. Huang, Y. Pan, Y. Wang, G. Su, J. Chen, *Energy Convers. Manage.* 121 (2016) 186–193.
- [18] F. Bonaccorso, L. Colombo, G. Yu, M. Stoller, V. Tozzini, A. C. Ferrari, R. S. Ruoff, V. Pellegrini,

Science 347 (2015) 1246501.

[19] S. Liang, L. K. Ang, Phys. Rev. Appl. 3 (2015) 014002.

[20] S. Misra, K. M. Upadhyay, S. K. Mishra, J. Appl. Phys. 121 (2017) 065102.

[21] S. K. Mishra, M. U. Kahaly, S. Misra, Int. J. Therm. Sci. 121 (2017) 358.

[22] S. Liang, B. Liu, W. Hu, K. Zhou, L. K. Ang, Sci. Rep. 7 (2017) 46211.

[23] X. Zhang, Y. Pan, J. Chen, IEEE Trans. Electron Devices 64 (2017) 4594–4598.

[24] W. Shi, J. Zhu, M. Han, Z. Sun, Y. Guo, Applied Energy 252 (2019) 1134442.

[25] M. Ni, Int. J. Hydrogen Energy. 37(8) (2012) 6389–6399.

[26] J. Larminie, A. Dicks, Fuel Cell Systems Explained. New York: Wiley, 2000.

[27] J. Udagawa, P. Aguiar, N. P. Brandon, J. Power Sources 166 (2007) 127–36.

[28] T. Liao, B. Lin, Y. Wang, Acta Physica Sinica 68 (2019) 187901.

[29] J. H. Lee, I. Bargatin, N. A. Melosh, R. T. Howe, Appl. Phys. Lett. 100 (2012) 173904.

[30] Y. Chen, S. Deng, N. Xu, J. Chen, Appl. Phys. Lett. 116 (2020) 063902.

[31] H. Feng, L. Chen, Z. Xie, F. Sun, J. Power Sources 286 (2015) 406–413.

List of Tables

Table 1. The operating conditions and parameters of the coupled system [8, 9, 27].

Table 2. The effects of the collector's work function on the parametric optimal characteristics of the SOFC-GTEC coupling system.

List of Figures

Fig. 1. (a)The schematic diagram of a SOFC-GTEC coupled system and (b) the energy band diagram of GTEC.

Fig. 2. The curves of (a) the maximum power density P_{\max} and the maximum efficiency η_{\max} , (b) the optimized voltages $V_{T,P}$ and $V_{T,\eta}$, (c) the optimized current densities $J_{F,P}$ and $J_{F,\eta}$, and (d) the optimized area ratios α_p and α_η varying with the temperature T_F .

Fig. 3. The curves of (a) the power output density P and the efficiency η , (b) the temperature T_F of the SOFC and the open-circuit voltage $V_{T,oc}$ of the GTEC varying with the current density J_F .

Fig. 4. The curves of (a) the power output density P and the efficiency η , (b) the temperature T_F of the SOFC and the shorted current density $J_{F,SC}$ of the GTEC varying with voltage V_T .

Fig. 5. The 3D graphs of (a) temperature T_F , (b) current density J_T , (c) power density P , and efficiency η varying with voltage V_T and current density J_F .

Fig. 6. The curves of (a) the power output density P and the efficiency η varying with J_F , (b) the power output density P varying with the efficiency η , where the voltage V_T is optimized.

Table 1. The operating conditions and parameters of the coupled system [8, 9, 27].

Parameter	Value
Fuel composition pressures, p_{H_2} (atm); p_{H_2O} (atm)	0.97; 0.03
Air composition pressures, p_{O_2} (atm); p_{N_2} (atm)	0.21; 0.79
Cathode and anode exchange current densities, $J_{e,c}$; $J_{e,a}$ ($A \cdot cm^{-2}$)	0.53; 0.20
Cathode and anode limiting current densities, $J_{L,c}$; $J_{L,a}$ ($A \cdot cm^{-2}$)	2.16; 2.99
Heat transfer coefficient, U_E ; U_C ($W \cdot cm^{-2} \cdot K^{-1}$)	0.20
Richardson constants, A_E ($A \cdot cm^{-2} \cdot K^{-3}$); A_C ($A \cdot cm^{-2} \cdot K^{-2}$)	0.01158; 120
Ambient temperature, T_A (K)	300

Table 2. The effects of the collector's work function on the parametric optimal characteristics of the SOFC-GTEC coupled system.

ψ_C (eV)	P_{\max} (W·cm ⁻²)	$T_{F,P}$ (K)	$J_{F,P}$ (A·cm ⁻²)	$V_{F,P}$ (V)	$V_{T,P}$ (V)	η_{\max}	$T_{F,\eta}$ (K)	$J_{F,\eta}$ (A·cm ⁻²)	$V_{F,\eta}$ (V)	$V_{T,\eta}$ (V)
2.00	1.01	1276	1.88	0.412	0.783	0.579	1050	0.628	0.746	1.39
1.80	1.08	1248	1.94	0.389	0.917	0.579	1050	0.629	0.746	1.31
1.60	1.16	1236	1.98	0.366	1.08	0.579	1051	0.641	0.741	1.22

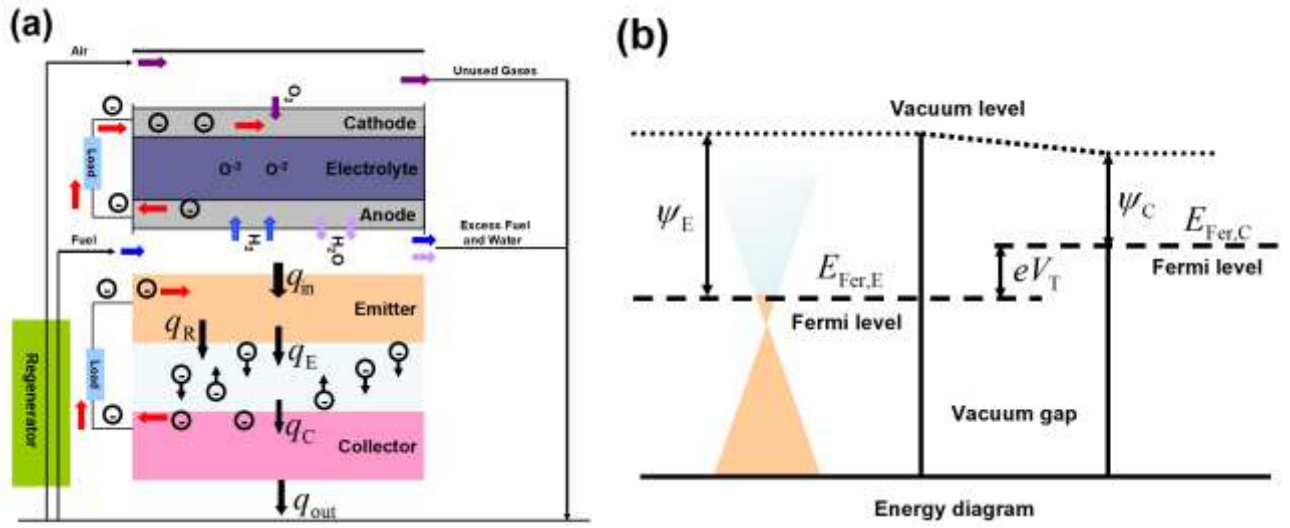


Fig. 1. (a)The schematic diagram of a SOFC-GETC coupled system and (b) the energy band diagram of GETC.

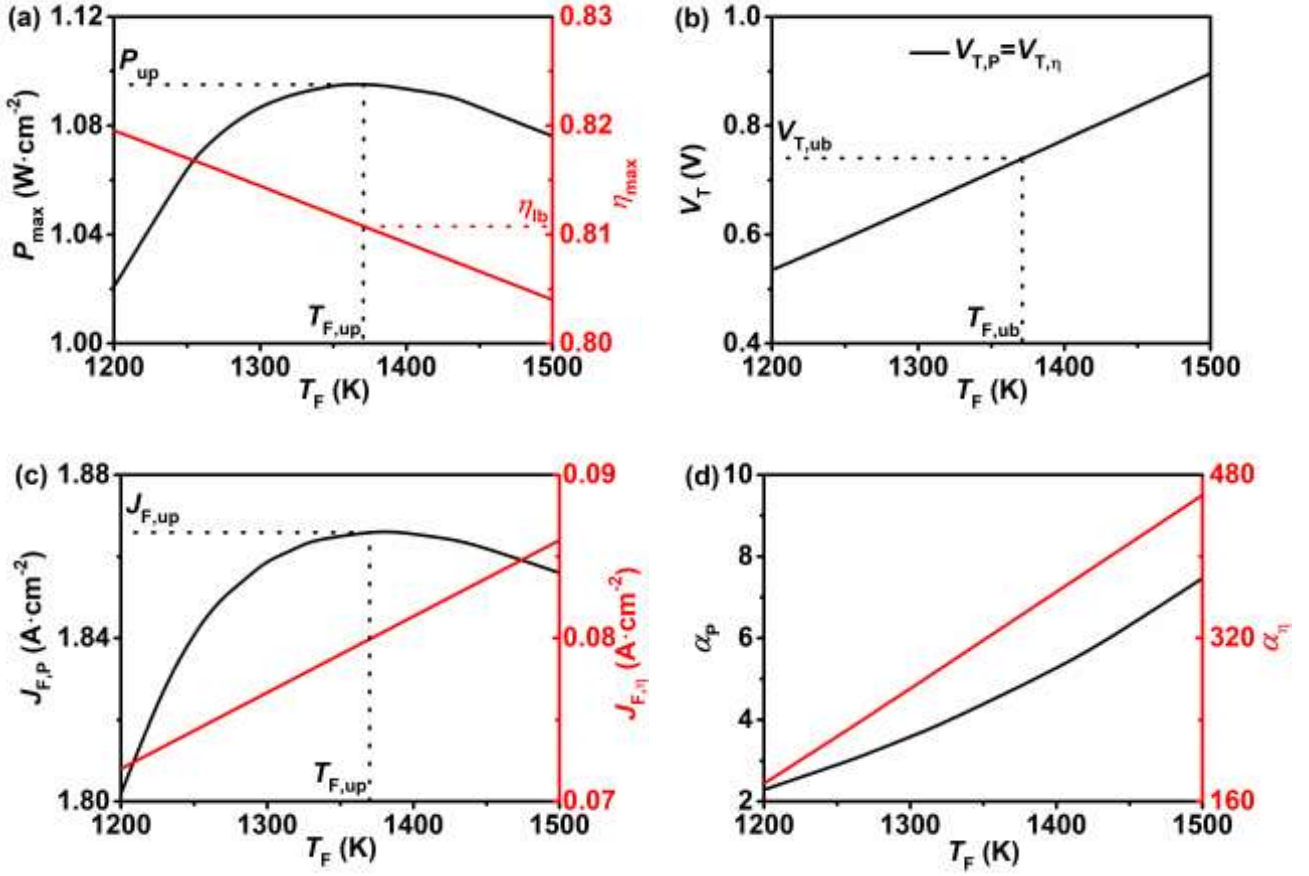


Fig. 2. The curves of (a) the maximum power density P_{\max} and the maximum efficiency η_{\max} , (b) the optimized voltages $V_{T,P}$ and $V_{T,\eta}$, (c) the optimized current densities $J_{F,P}$ and $J_{F,\eta}$, and (d) the optimized area ratios α_p and α_η varying with the temperature T_F .

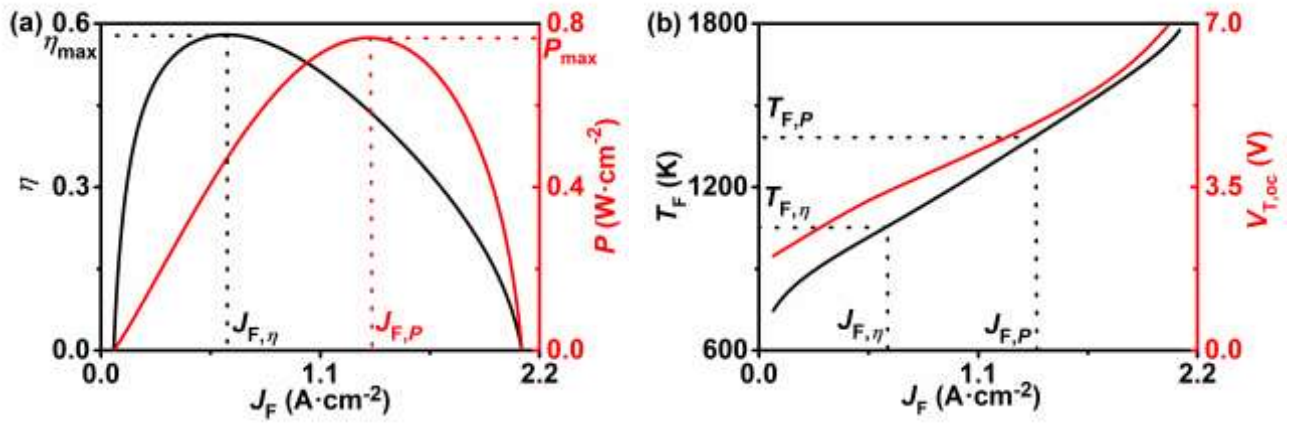


Fig. 3. The curves of (a) the power output density P and the efficiency η , (b) the temperature T_F of the SOFC and the open-circuit voltage $V_{T,OC}$ of the GTEC varying with the current density J_F .

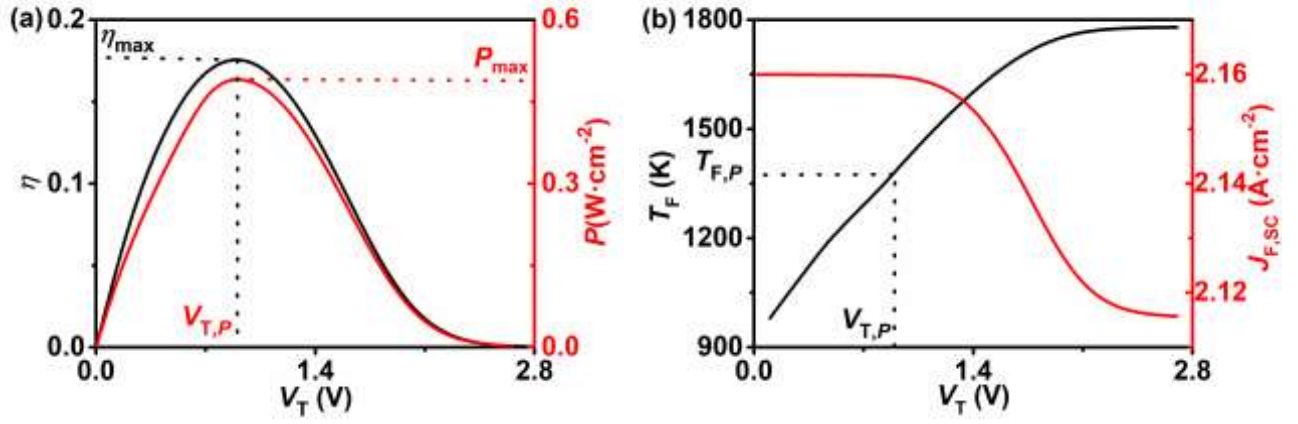


Fig. 4. The curves of (a) the power output density P and the efficiency η , (b) the temperature T_F of the SOFC and the shorted current density $J_{F,SC}$ of the GTEC varying with voltage V_T .

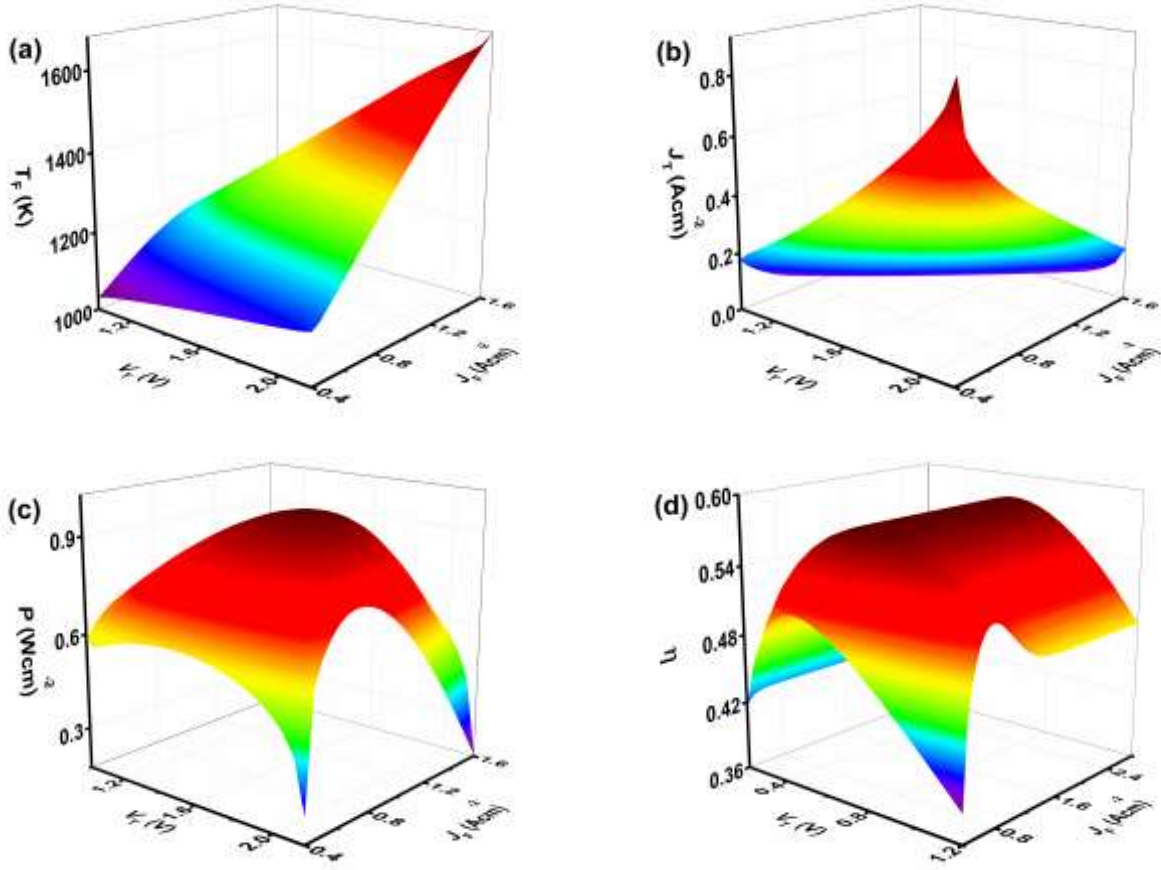


Fig. 5. The 3D graphs of (a) temperature T_F , (b) current density J_T , (c) power density P , and efficiency

η varying with voltage V_T and current density J_F .

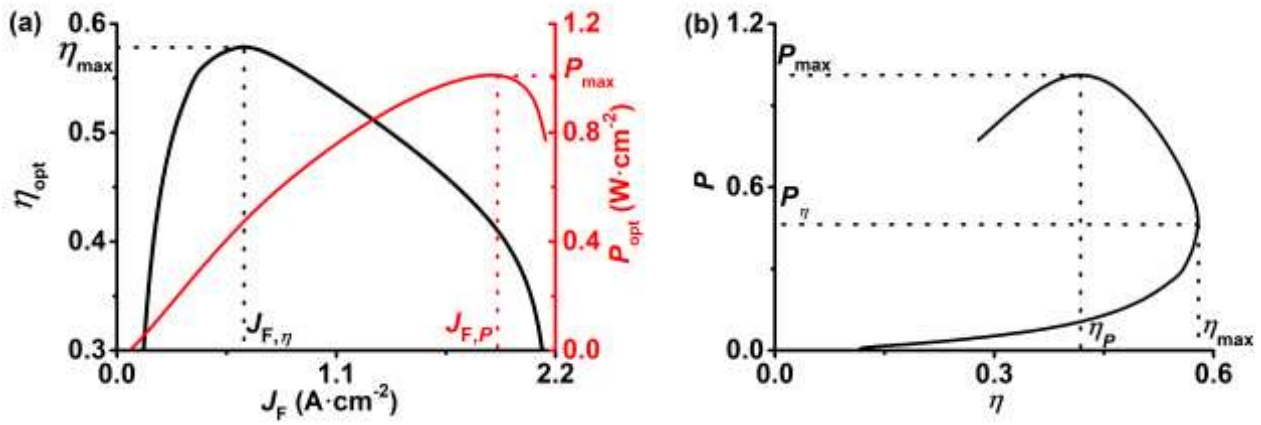


Fig. 6. The curves of (a) the power output density P and the efficiency η varying with J_F , (b) the power output density P varying with the efficiency η , where the voltage V_T is optimized.